Ocean Engineering 237 (2021) 109638

Contents lists available at ScienceDirect

Ocean Engineering

journal homepage: www.elsevier.com/locate/oceaneng

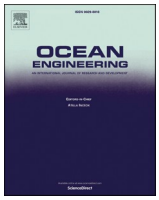

Effects of mooring line breakage on dynamic responses of grid moored fish farms under pure current conditions

Hui Cheng [a,*], Lin Li [a], Muk Chen Ong [a], Karl Gunnar Aarsæther [b], Jaesub Sim [a]

[a] Department of Mechanical and Structural Engineering and Materials Science, University of Stavanger, 4036, Stavanger, Norway
[b] Department of Technology and Safety, UiT the Arctic University of Norway, 9037, Tromsø, Norway

ARTICLE INFO

Keywords:
Norwegian fish farm
Mooring line breakages
Mooring system
Numerical simulation
Grid moored fish farm

ABSTRACT

Due to the lack of sheltered area, Norwegian fish farms are expanding to more exposed and remote sites. The severe environmental conditions in exposed sites can increase the risk of structural failure during aquaculture operations. In the present study, the program FhSim is employed to conduct time-domain simulations to investigate structural responses of a single-cage and 1 × 4 multi-cage fish farm due to breakages in mooring lines. The influences on the tension distribution in the mooring system and the displacement of the buoys due to breakage at different mooring lines are analysed in detail. Based on the analysis, a method to identify the broken mooring line and to predict the maximum tension increment in the remaining mooring lines is proposed. The results indicate that the breakage at one mooring line is unlikely to cause a progressive collapse of the fish farm immediately when the current velocity is less than 0.5 m/s. However, these breakages may cause structural collapses and fish escapes when the current and waves increase. In order to prevent fish escapes, suggestions to improve the mooring system design and recommendations for monitoring during operations are given.

1. Introduction

The expanding global population together with stagnation in capture fisheries is driving the demand for aquaculture products. According to the report by the Food and Agriculture Organization of the United Nations (FAO, 2020), the global population is expected to reach nine billion by the middle of the twenty-first century. Food production from aquaculture is expected to exceed traditional capture fisheries in 2021 (Fredheim and Reve, 2018), and will be the main contributor to global food production as the population increases. FAO (2020) statistics show that marine finfish production is dominated by Atlantic Salmon (*Salmo salar*), and Norwegian production accounts for more than 50 % of the global salmon production. While the Norwegian coast provides a favourable production environment, the success of marine aquaculture in Norway is based on regulations and design guidelines which are established to support sustainable aquaculture. Fish farming in Norway is regulated through production licenses issued and regulated by the Directorate of Fisheries based on the Aquaculture Act (Norwegian Directorate of Fisheries, 2005). The regulation limits the number of aquaculture farms, but also impose requirements on planning, design and operation in order to reduce adverse side effects such as waste, parasites and escape of farmed salmon.

Escapes of farmed fish can cause an economic loss for fish farmers, threat the wild fish populations, and reduce the societal acceptance of the aquaculture industry. Fig. 1 shows the production of farmed salmon and the number of escaped salmon in Norway in the period between 2000 and 2019 (Statistics Norway, 2020). The salmon production grows rapidly during the years 2000–2013, which lead to an increase in the number of fish escapes, especially before 2006. According to Moe Føre and Thorvaldsen, 2021, 92 % of fish escapes were triggered by technological factors, such as submergence of the net top and holes in nettings. The Norwegian Standard NS 9415 (Standards Norway, 2009) on the design, operation and installation of fish farms was introduced in 2004 (Berstad et al., 2004) and compliance was ensured through the Aquaculture Act. This technical standard was revised in 2009 and enforced correspondingly in 2011. The implementation of NS 9415 increases technological investments and reduces the number of escaped fish. According to the report by Moe Føre et al., 2019, 82 % of fish escapes in the period 2014–2018 happened during normal operations, such as handling weights and netting (in preparation for delousing). In the last decade, human and organisational factors during in-situ operations, instead of technological factor, have been identified as dominant

* Corresponding author. University of Stavanger: Universitetet i Stavanger, Kjell Arholms gate 41, 4036, Stavanger, Rogaland, Norway.
E-mail address: hui.cheng@uis.no (H. Cheng).

https://doi.org/10.1016/j.oceaneng.2021.109638
Received 12 February 2021; Received in revised form 30 June 2021; Accepted 6 August 2021
Available online 17 August 2021

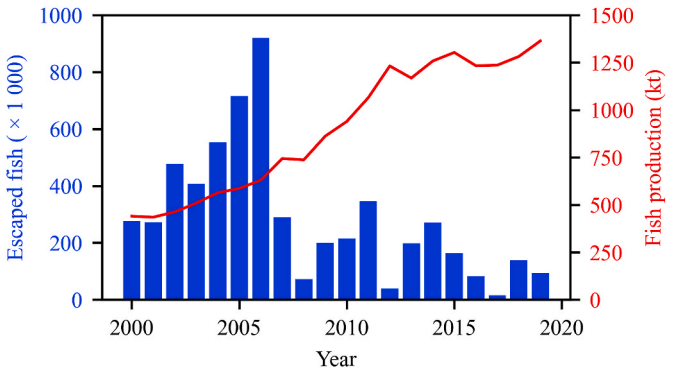

Fig. 1. Fish production and number of escaped fish in Norway from 2000 to 2019. (Statistics Norway, 2020).

underlying causes for fish escapes (Thorvaldsen et al., 2015, 2018).

Fish farming is a complex process with various in-situ operations, such as delousing process, changing/cleaning netting and transfer of fish. These operations usually involve a number of operators, different types of equipment and well boats (Høyli, 2016). During operations, well boats can bring substantial forces on mooring lines, as they are moored to aquaculture structures. According to the research by Shen et al. (2019), loads on anchor lines can increase 40 % due to the existence of well-boats, even under modest current velocities of 0.3 m/s. Furthermore, underwater structural failures, such as tears on netting and mooring line breakage, may be difficult to detect during operations. These unaware structural failures may lead to fish escapes. Tang et al. (2019) investigated structural responses of a single-cage fish farm due to mooring line breakages. The results indicated that tensions in the remaining mooring lines could increase up to 1.75 times compared to those under intact condition. In order to prevent fish escapes, a quick approach to detect and identify structural failures during operations is necessary (Yang et al., 2020a). This quick approach needs comprehensive analyses in the design phase on the structural responses of fish farms due to various structural failures. When the fish farms are established in exposed and remote areas, understanding how the surface visible parts of the structure are influenced by the combination of current and broken lines can lead to fast identification of failures by remote operators. However, to the best of our knowledge, such analyses are rarely reported in literature.

A marine fish farm is built to support the containment netting with components, floater, weight system, interconnecting ropes, mooring lines, anchor and supporting buoys. A typical Norwegian marine fish farm is illustrated in Fig. 2. These structures have complex topology regarding the interconnection of structure members, and combinations of elastic, stiff and permeable structures. A comprehensive model is needed to analyse such structures, and considerable research effort has been spent to analyse the physical effects of fish farm structures. Endresen et al. (2013) developed a numerical tool to calculate the total drag force and deformation of a fish farm under complex sea conditions. Zhao et al. (2013a) employed a porous media model to simulate the flow through a net panel and showed that the velocity reduction downstream from one net panel is 11 %. Bi et al. (2014) proposed a coupled fluid-structure model to study the weak effect after a fish cage and showed that the maximum velocity reductions downstream from a single fish cage are 17.5 %. Zhao et al. (2013b) established a numerical model for multi-cage fish farm using a porous media model and showed 69 % of velocity reduction when the flow passed through 4 cages. Gutiérrez-Romero et al. (2020) comprehensively analysed a fish farm under combined wave and current conditions using a fluid-structure interaction method. All the above studies proved that the numerical method is accurate enough to predict the structural responses of a fish farm under various current and wave conditions. Thus, the effects of mooring line breakage on dynamic responses of grid moored fish farms are investigated through numerical simulations in the present study.

With complex in-situ operations which can lead to increased loads on different structure members, it is important to understand how breakage in any part of the fish farm will affect the response and load distribution. In the present study, the structural responses of a fish farm due to mooring line breakages under operational conditions (*i.e.*, current velocity is less than 0.5 m/s) are comprehensively analysed. In Sections 2 and 3, the numerical model and the description of fish farms are presented, respectively. Results and detailed analysis are given in Section 4. Finally, the results of this study are summarised in the conclusions.

2. Numerical model

2.1. FhSim framework

In the present study, numerical models of full-scale fish farms are prepared in FhSim, which is a modular analysis program developed by SINTEF Ocean. This program has been validated with experiments and extensively used for the analysis of fish farms (Endresen et al., 2013; Endresen et al., 2014; Reite et al., 2014; Su et al., 2019), and the validations showed satisfactory results for current velocities less than 0.7

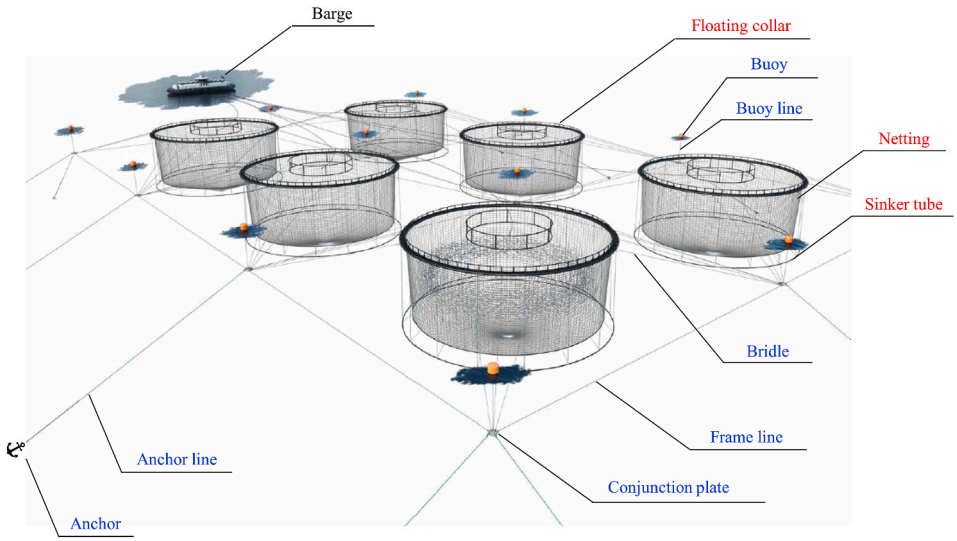

Fig. 2. Illustration of a typical Norwegian fish farm with 2 × 3 fish cages (AKVA group, 2020).

m/s, with a discrepancy between the numerical and experimental results in the region of 7 %.

Fig. 3 represents how variables, *i.e.*, displacement, velocity and force, are transferred across the objects representing a fish farm during numerical analysis in FhSim. A newly compiled module (the "mooring system" in Fig. 3) was implemented in the existing program to represent a conventional "grid-mooring system". By implementing the new module, the initial setup and the exchange of forces become efficient since all the objects in the mooring system are packed into one single module. This new module has also been successfully applied in the numerical simulations of a 2 × 4 multi-cage fish farm by Sim et al. (2021). FhSim supports the use of several different integration methods, including Euler method, Heun's method and Runge-Kutta method. In this study, the Runge-Kutta method with variable time steps is used for numerical integration. The mooring system and netting are modelled as collections of interconnected discrete rigid bodies and mass points, respectively. The rigid bodies, or elements, that comprise the mooring system are connected by constraint forces that replicate a linear strain-stress relationship between the elements with an explicit elastic Baumgarte stabilization technique (Skjong et al., 2021). The mass of the netting are lumped into mass points, and interconnected as triangular elements where structural forces are calculated along the netting twines as in and distributed evenly to the three interconnected mass points (Priour, 1999). The response of the structure is calculated in the time domain with equations:

$$[\boldsymbol{M}]\ddot{\boldsymbol{q}} = \boldsymbol{F}_s(\boldsymbol{q}) + \boldsymbol{F}_g + \boldsymbol{F}_b + \boldsymbol{F}_h(\boldsymbol{q}, \dot{\boldsymbol{q}}) \tag{1}$$

where $\boldsymbol{q}$ is the time-dependent vector of nodal displacements, $\boldsymbol{M}$ is the mass matrix, $\boldsymbol{F_s}$ is the force vector for the structural forces acting on the mass, $\boldsymbol{F_g}$ is the force vector due to gravity, $\boldsymbol{F_b}$ is the force vector due to buoyancy, and $\boldsymbol{F_h}$ is the force vector for the hydrodynamic forces. By solving Eq. (1), the cage net deformations can be acquired.

2.2. Structural model

The netting in the present study is discretised based on the triangular element method proposed by Priour (2013). The triangular elements are interconnected through nodes, and the total mass of the netting is distributed onto these nodes. The environmental loads acting on a triangular element, are computed as the total loads acting on individual twines within the triangular element and distributed onto its corresponding nodes (Enerhaug et al., 2012).

The buoy is modelled as vertical circular cylinders with a conical bottom. It is given 5 degrees of freedom (DOF), where rotation around its vertical axis is omitted (Fredriksson et al., 2014).

Anchor lines, frame lines, bridles and other components with cable-like properties are modelled using discrete rigid body elements combined into cables with a inter element dynamic constraint formulation on axial and angular displacements. The sinker tube is modelled by the same discrete element type as used in the cable, but with two endpoints connected to create a circle. The tension in a cable-like element is calculated as a constraint force (Skjong et al., 2021), where the parameters of the Baumgarte Stabilization between elements are selected to give a linear material response:

$$|F| = EA\frac{l - l_0}{l_0} \tag{2}$$

where E is Young's modulus of the material, A is the section area of the cable, l_0 is the unstretched length of the cable and l is the length of the cable. The mathematical and theoretical descriptions for the cable-like elements in FhSim are given by Johansen (2007) and Skjong et al. (2021).

The floating collar is modelled as a flexible continuous circular ring using beam elements. It is divided into sections, and for each section, the radial and vertical responses are calculated using the Euler beam equations (Eq. (3)).

$$\begin{aligned} F_R(s,t) &= m\frac{\partial^2 v}{\partial t^2} + EI\left(\frac{\partial^4 v}{\partial s^4} + \frac{1}{R^2}\frac{\partial^2 v}{\partial s}\right) \\ F_Z(s,t) &= m\frac{\partial^2 z}{dt^2} + EI\frac{\partial^4 z}{ds^4} \end{aligned} \tag{3}$$

where v and z are the radial and vertical responses of the floater respectively, m is the mass per unit length of the floater, EI is the bending stiffness of the floater, F_R is the radial force on the floater per unit length and F_Z is the vertical force on the floater per unit length.

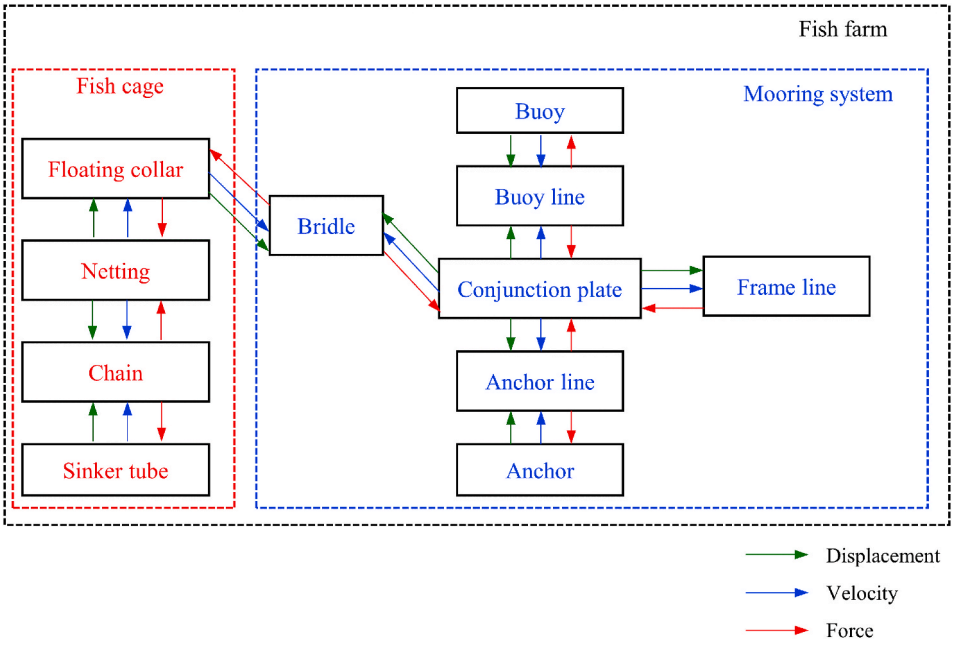

Fig. 3. Topological relationship for the different components in a fish farm.

2.3. Hydrodynamic model

In this study, the hydrodynamic forces acting on the triangular element is calculated by integrating the force on individual twines within the triangular element. Individual twine is regarded as a smooth cylinder, and its hydrodynamic force is calculated using quadratic drag formulation. In case of inclined twines due to the geometry or deformation of the cage, the hydrodynamic forces on twines are decomposed into normal force $\boldsymbol{F_N}$ and tangential force $\boldsymbol{F_T}$, as shown in Eq. (2).

$$\boldsymbol{F_N} = 0.5C_N\rho A|\boldsymbol{U_N}|\boldsymbol{U_N}\boldsymbol{F_T} = 0.5C_T\rho A|\boldsymbol{U_T}|\boldsymbol{U_T} \quad (4)$$

where, $\boldsymbol{U_N}$ and $\boldsymbol{U_T}$ are the normal and tangential components of the relative flow velocity for each twine, respectively. C_N, C_T are the normal and tangential drag coefficients, respectively, and are dependent on Reynolds number (Re). A is the reference area which is the product of the length and the diameter of a twine. C_T is assigned with a constant value of 0.01 for all Re, and C_N is taken from the experimental data as a seventh order polynomial function of the logarithmic Re, which is limited in the range of 32 and 10^4 (Kristiansen and Faltinsen, 2012; Cheng et al., 2020a).

$$\begin{aligned} C_N = &-78.46675 + 254.73873(log_{10}Re) - 327.8864(log_{10}Re)^2 \\ &+ 223.64577(log_{10}Re)^3 - 87.92234(log_{10}Re)^4 + 20.00769(log_{10}Re)^5 \\ &- 2.44894(log_{10}Re)^6 + 0.12479(log_{10}Re)^7 \end{aligned} \quad (5)$$

where $Re = \frac{U_{net}d_t}{\nu}$, $U_{net} = \frac{\sqrt{2-S_n}}{\sqrt{2(1-S_n)}}U_\infty$, d_t is the diameter of a twine, ν is the kinematic viscosity of water, S_n is solidity ratio, and U_∞ is the incoming current velocity.

3. Description of the fish farm system

3.1. Fish cage description

This study focuses on typical Norwegian fish cages which include a double-pipe floating collar, a cage net (cylindrical net structure with conical bottom), ropes for supporting the weight system, chains (connecting cage net and sinker tube), a sinker tube and a centre point weight. In order to keep fish cages at targeted locations, a grid mooring system that includes anchors, buoys, connection plates, bridles, buoy lines, anchor lines and frame lines, should be properly designed according to the environmental conditions. Fig. 2 illustrates how these components are interconnected in a typical Norwegian fish farm. The topological relationship of the aforementioned components in numerical simulations is shown in Fig. 3. The dimensions and physical properties of the main components used in this paper are listed in Table 1.

3.2. Single-cage fish farm

Fig. 4 shows an overview of the single-cage fish farm. The mooring lines are named following matrix style, reflecting the matrix-like structure of the grid mooring system. "Mx" represents the mooring lines along X-axis. The first digit of the index number after "Mx" represents the index of the line in the Y-direction, and the second digit represents the index of the line in the X-direction. The "My" lines along Y direction are labelled in a similar fashion. Since this model only contains one fish cage, the mooring lines whose name ends with number "1" are frame lines, and the rest are anchor lines. The labels of buoys follow the same matrix fashion starting with "B", with the following two numbers indicating the location in the mooring frame.

Fig. 5 shows the time series of the numerical results for this single-cage fish farm with a current velocity of 0.5 m/s and current direction $\theta = 0°$. Although the simulation is under pure current conditions, oscillations are observed in the numerical results. These oscillations come from the nonlinearity of the system, which is also reported by Antonutti et al. (2018) and Cheng et al. (2021). The oscillations are deemed acceptable, as the standard deviation for the time-series force over the last 100 s is 3.1 % of the mean force. The time-series results indicate that the simulation reaches the steady-state after 300 s. Hereafter, the tensions in mooring lines and displacements of buoys are time-averaged under steady-state conditions. Fig. 6 shows the deformation of the single-cage fish farm in a steady-state condition. Due to the pre-tensions in mooring lines, the displacements of other components, such as floating collar and mooring lines, are unnoticeable.

Table 1
Dimensions and properties of the fish cage.

Component	Parameter	Value	Unit
Floating collar	Inside diameter	51	m
	Outside diameter	53	m
	Section diameter	0.25	m
	Wall thickness	28.4	mm
	Young's modulus	0.9	GPa
	Linear density	81	kg/m
Netting	Section diameter	2.5	mm
	Mesh length	25	mm
	Density	1125	kg/m^3
	Young's modulus	0.1	GPa
	Vertical cylinder depth	15	m
	Conical bottom depth	28	m
Sinker Tube	Tube diameter	51	m
	Section diameter	0.25	m
	Center point weight	100	kg
	Linear density	51	kg/m
Mooring line	Initial length of anchor line	120	m
	Initial length of frame line	100	m
	Section diameter	0.05	m
	Young's modulus	1	GPa
	Density	1100	kg/m^3
Buoy	Diameter	2	m
	Vertical cylinder depth	1	m
	Conical bottom depth	2	m

3.3. 1x4 multi-cage fish farm

Fig. 7 shows the plan view of the 1x4 multi-cage fish farm. The labels of mooring lines and buoys follow the same rule as the single-cage fish farm. The longest axis of this fish farm is along the X-axis. As the four fish cages are arranged along X-axis, these mooring lines along X-axis whose name ends with a number between 1 and 4 are frame lines, and these mooring lines along Y-axis whose name ends with number "1" are frame lines. The fish cage is named Cage1 to Cage4 from left to right. The labels of buoys also follow the matrix style.

Fig. 8 shows the time series of the numerical results for this 1x4 multi-cage fish farm when current velocity is 0.5 m/s and current direction $\theta = 0°$. Oscillations of drag force are also observed in the numerical results. The standard deviation for the time-series drag force over the last 100 s is up to 5.3 % of the mean drag force for the four cages. Due to the existence of the upstream fish cags, the current velocity for the downstream fish cage is reduced. The fish cage located downstream, *e.g.*, Cage2, experiences a smaller current velocity compared to Cage1. Thus, Cage2 experience a smaller current load. The smaller current load makes Cage2 has less deformation and larger cultivation volume than Cage1. Thus, the volume and drag force of the four fish cages are different due to the different experienced current velocities. The mechanism that causes the current velocity reduction in the downstream location is the weak effect. The detailed explanations and discussions for the weak effect can refer to Cheng et al. (2020b) and Sim et al. (2021). Here, only the final expression for the current velocity in the rear of a fish cage, $U_{rear}(x, y)$, is presented:

$$U_{rear}(x,y) = \left(1 - V_{decay}\right)U_\infty \quad (6)$$

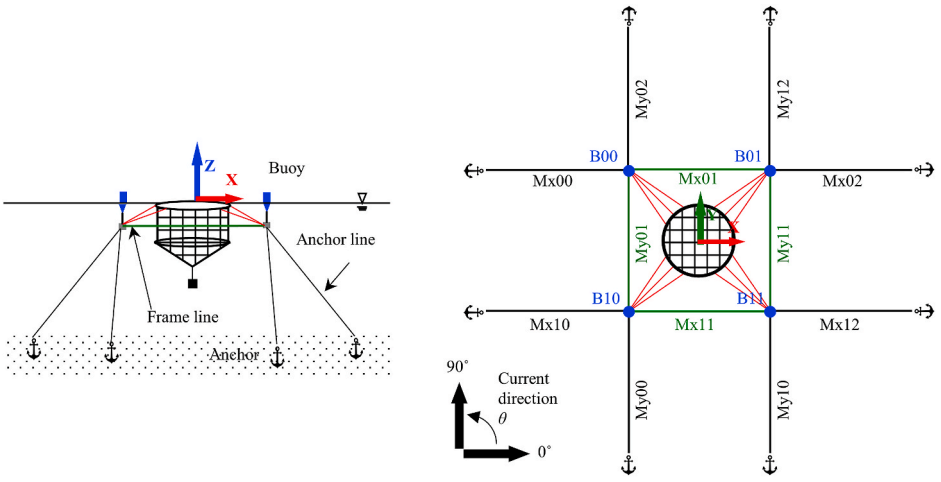

Fig. 4. Overview of a single-cage fish farm. The current direction is defined as 0° when the current heads to X+.

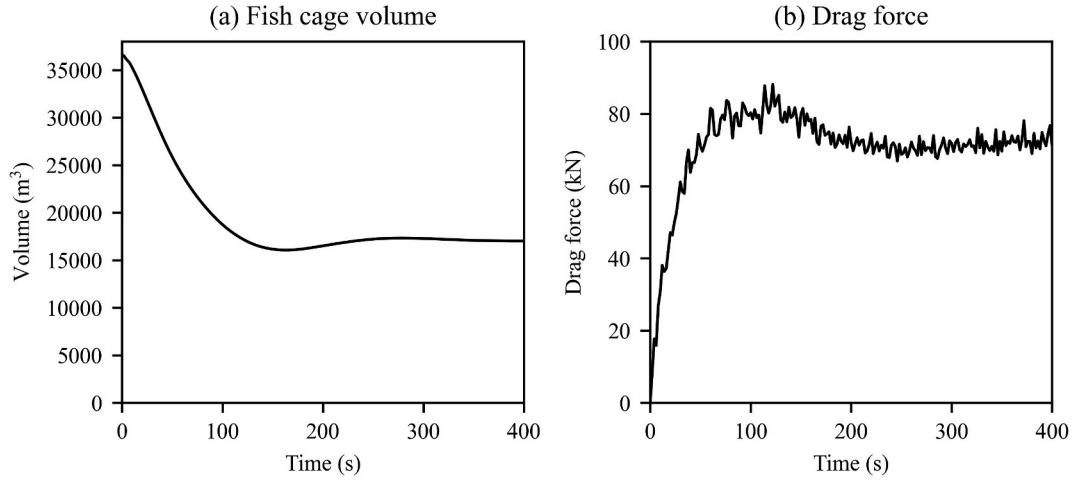

Fig. 5. Time-series results for the cultivation volume and drag force on fish cage when current velocity is 0.5 m/s and current direction is 0°.

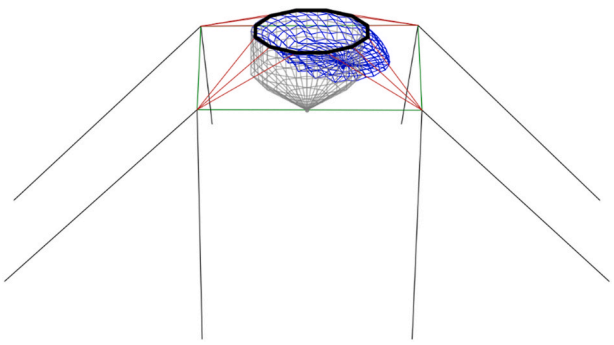

Fig. 6. The deformation of a fish cage when current velocity is 0.5 m/s and current direction is 0°. For the netting, the grey lines show the undeformed fish cage, and the blue line is the deformed fish cage. (For interpretation of the references to colour in this figure legend, the reader is referred to the Web version of this article.)

$$V_{decay} = V_r \cdot \frac{S_n}{0.25} \sqrt{exp\left(-\frac{x/D - 1.5}{25}\right)} \tag{7}$$

$$\begin{aligned} V_r = {} & 0.1201 + 0.2414cos(\omega y/D) + 0.0115cos(2\omega y/D) - 0.0644cos(3\omega y/D) \\ & + 0.0030cos(4\omega y/D) + 0.0294cos(5\omega y/D) - 0.0058cos(6\omega y/D) \\ & - 0.0149cos(7\omega y/D) \end{aligned} \tag{8}$$

where U_∞ is the incoming current velocity for this fish cage, the constant $\omega = 2.692$ is found by a fit of the experimental data from Gansel et al. (2012), D is the diameter of this fish cage, and S_n is the solidity of the netting. (x, y) is the coordinate in a local coordinate system where the X+ axis is aligned with the current direction, Z+ is opposite to gravity, and Y-axis is perpendicular to the X-axis and Z-axis. As $U_{rear}(x, y)$ is only meaningful downstream of a fish cage, x is larger than $0.5D$. The assumption proposed by Sim et al. (2021) that the influence width of the wake is approximately twice of the fish cage diameter is adopted in this study. Hereby, $-1 < y/D < 1$.

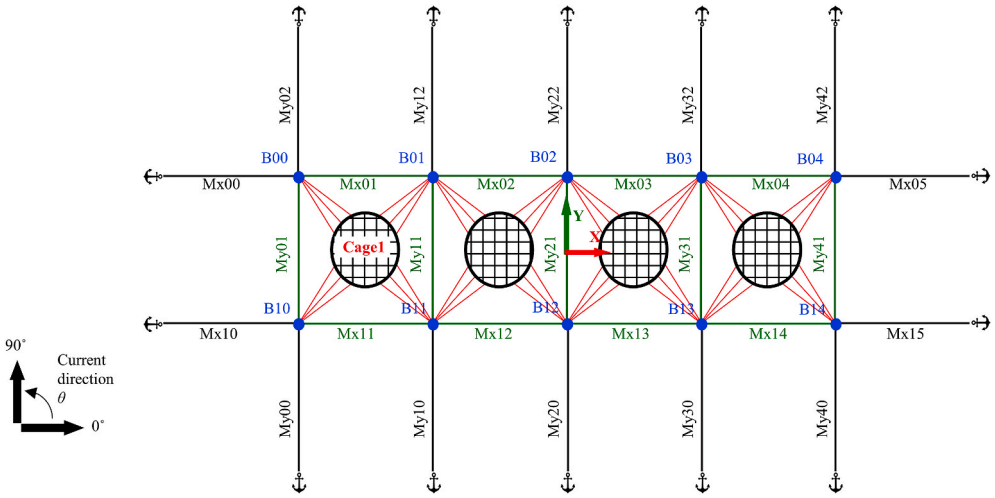

Fig. 7. Top view of the 1 × 4 multi-cage fish farm.

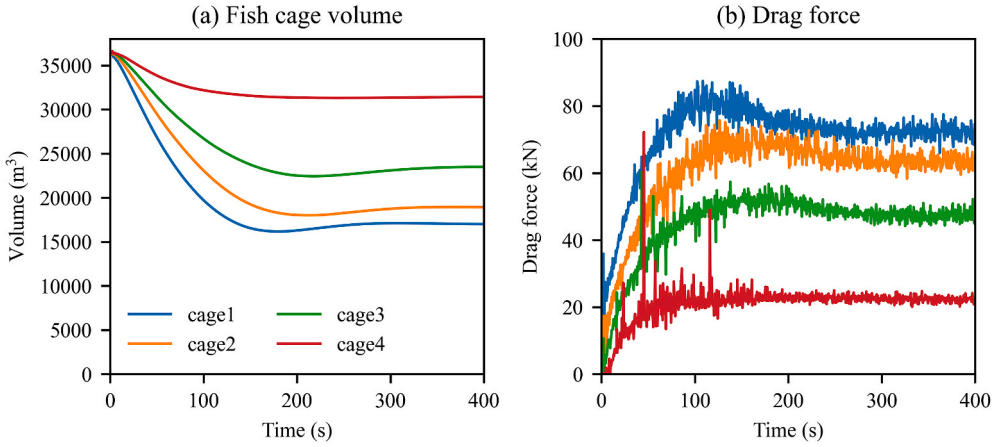

Fig. 8. Time-series results for the cultivation volume and drag force on fish cages when current velocity is 0.5 m/s and current direction is 0°.

Table 2
Summary of simulations cases.

		Single-cage fish farm	1 × 4 multi-cage fish farm
Intact cases	Current velocity	0.5 m/s	0.5 m/s
	Current direction	0°–360°	0°–360°
	Number of cases	36	36
Structural-failure cases	Current velocity	0.5 m/s	0.5 m/s
	Current direction	0°–360°	0°–360°
	Position of breakage	Mx*ij* ($i = 0, 1; j = 0, 1, 2$)	Mx*ij* ($i = 0, 1; j = 0, 1, 2, 3, 4, 5$)
		My*ij* ($i = 0, 1; j = 0, 1, 2$)	My*ij* ($i = 0, 1, 2, 3, 4; j = 0, 1, 2$)
	Number of cases	36 × 12 = 432	36 × 27 = 972

3.4. Environmental conditions

According to the report by Halwart et al. (2007), most of the conventional fish farms are located at sheltered sites. The sheltered site, according to the Norwegian Standards (Standards Norway, 2009), refers to the location with a significant wave height of 0–0.5 m and a peak wave period of 0–2 s. According to the previous study by Shen et al. (2018), the waves at the sheltered sites can only contribute up to 10% of the tension forces in mooring lines when the current velocity is 0.5 m/s. As the present study focuses on the structural responses of the conventional fish farms under operational conditions, wave-induced forces are insignificant compared to current-induced forces. Thus, the waves are not included in the present numerical simulations. Pure current conditions with an assumption that the current is steady and uniform over the entire water depth are applied to all the cases. The applied current velocity is 0.5 m/s which corresponds to the velocity for a moderately exposed site, and the water depth is 80 m. As the current direction may vary in fish farms, current directions from 0° to 360° with a 10° interval are considered.

3.5. Simulation of the mooring line breakages

In order to study line breakage, a function was implemented into the existing program, FhSim, to control where and when the breakage occurs in the mooring system. For these mooring line breakage cases, the simulations are conducted under an intact condition until it reaches a

steady-state condition, and then the constraint equations between the elements at the desired position are deactivated to simulate the mooring line breakage. Only one broken mooring line is included for each simulation case. For the single-cage fish farm, 12 breakage cases corresponding to the 12 mooring lines, *i.e.*, 8 anchor lines and 4 frame lines, are considered to investigate the influence of breakages at various positions. Together with the different current directions, there are $36 \times 12 = 432$ cases for the single-cage fish farm. Similarly, there are $36 \times 27 = 972$ cases for the 1×4 multi-cage fish farm. A summary of all the simulations in the present study is shown in Table 2. Regarding the measurements of structural responses, the tension force in all mooring lines, position of buoys, drag forces and cultivation volume of the fish cage are recorded before and after breakages occur. Because the two fish farms are symmetric with respect to the Y-axis and the X-axis, many interesting characteristics can be seen in the following results and discussion.

4. Results and discussion

4.1. Structural responses of a single-cage fish farm due to mooring line breakage

4.1.1. Tension distribution before mooring line breakage

Before the analysis of structural responses due to mooring line breakages, detailed results of tension distribution under intact conditions are presented. Fig. 9 presents the tension force in each mooring line when the current direction θ is 0°. The dashed lines represent pre-tensions in anchor lines and frame lines. The red colour shows that the tension in the anchor line is higher than the pre-tension, and the blue colour shows that the tension in the anchor line is lower than the pre-tension. According to the layout of this single-cage fish farm in Fig. 4, all the anchor lines in higher tensions, *i.e.*, Mx00, Mx10, My00 and My02 are located on the negative side of X-axis, which means they are the main contributors to hold the fish farms when the $\theta = 0°$. Tension forces in all the frame lines are much smaller than those in anchor lines. The tension in frame line My01, which is on the upstream side of the fish cage, is reduced compared to the pre-tension. When $\theta = 0°$, the drag force on the fish cage is acting along X+ direction, and this drag force is transferred to the mooring system through bridles (the red lines in Fig. 4). According to the equilibrium of forces, the tension in the front frame line My01 is reduced, and the tension in the rear frame line My11 is increased compared to their pre-tension. Together with Figs. 4 and 9, it can be seen that mooring lines which are symmetric with respect to the X-axis experience the same tension forces, such as Mx00 and Mx02 have the same value. When $\theta = 0°$, the environmental loads act along the axis of symmetry for this single-cage fish farm, and these loads can be symmetrically distributed among the mooring lines.

Fig. 10 shows the influence of different current directions on the tension distribution among anchor lines. This figure is plotted in a polar coordinate system, where the polar angle represents the current direction, and the radius represents the value of tension force. The tensions in anchor lines change with different current directions. Take Mx00 and Mx10 as an example. When $\theta = 0°$, the tension force in Mx00 and Mx10 are the same, which can also be seen in Fig. 9. With the increasing current direction, the tensions in Mx00 and Mx10 are reduced until $\theta = 180°$. The tension-deduction in Mx00 is first slower than that of Mx10 when $\theta < 90°$, and then faster than that of Mx10 when $\theta > 90°$. When $\theta = 180°$, the tensions in these two anchor lines are the same again. When $0° < \theta < 90°$, Mx10 is relatively located in front of Mx00, and thus Mx10 carries a higher proportion of the current-induced load on the fish farm. Hereby, the tension in Mx10 is larger than that in Mx00 when $0° < \theta < 90°$. For the current direction between 180° and 360°, the change of tensions in Mx00 and Mx10 follows an opposite trend compared to those when $0° < \theta < 180°$. The change of the tensions in other mooring lines can be interpreted in a similar way as with Mx00 and Mx10.

The tension distribution is symmetric when the environmental loads along the axis of symmetry for this single-cage fish farm. In addition to $\theta = 0°$, the symmetric tension distribution can also be observed when $\theta = n \times 45°$, where n is an integer. In Fig. 10, intersections of the curves occur when the tension distribution is symmetric. For $\theta = 45°$, 135°, 225° and 315°, these intersections can be observed by overlapping the two subplots for anchor lines in X and Y directions in Fig. 10. All the above symmetric characteristics are related to geometric characteristics of the single-cage fish farm. These symmetric characteristics can simplify fish farm design and structural analysis.

4.1.2. Tension distribution after mooring line breakage

When one of the mooring lines breaks, the environmental loads will be distributed among the remaining mooring lines, and consequently, the position of buoys may also change. The changes of tensions in the remaining mooring lines and positions of buoys, due to mooring line breakages, are presented in Fig. 11. The influence of mooring line breakages on the position of buoys will be discussed in Section 4.1.3. Fig. 11 is divided into six blocks in order to differentiate the influence of breakages in anchor lines and frame lines. Here we define anchor lines and frame lines as two mooring components. The names of the six

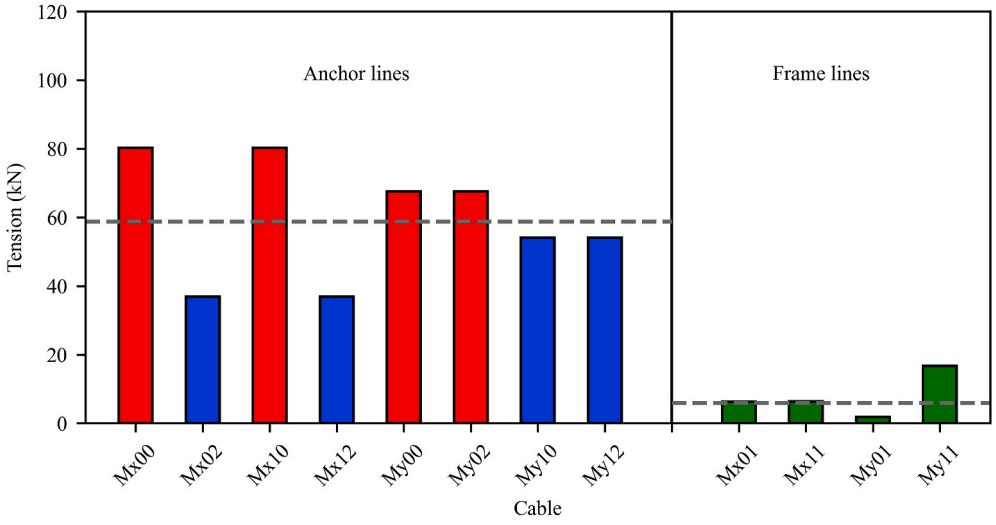

Fig. 9. Tension distribution in mooring lines, *i.e.,* anchor lines and frame lines, when the mooring system is in intact condition, current direction is 0° and current velocity is 0.5 m/s.

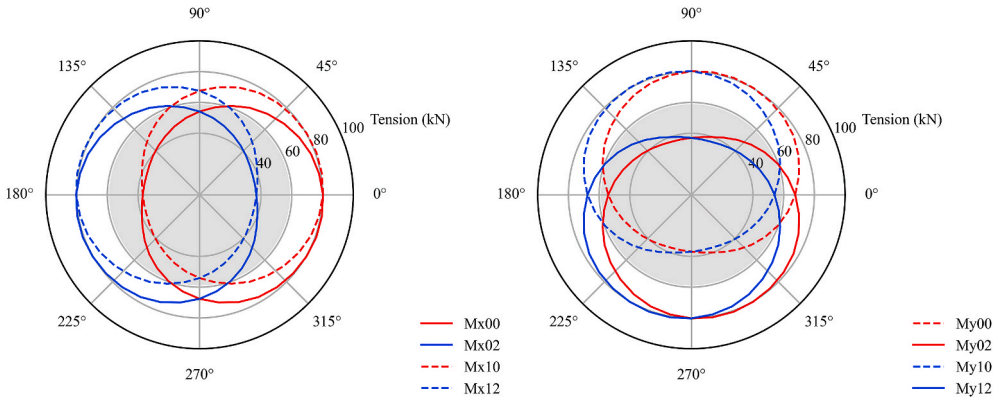

Fig. 10. Tension distribution in anchor lines under different current directions when the mooring system is in intact condition and current velocity is 0.5 m/s. The grey shadow represents pre-tension in anchor lines.

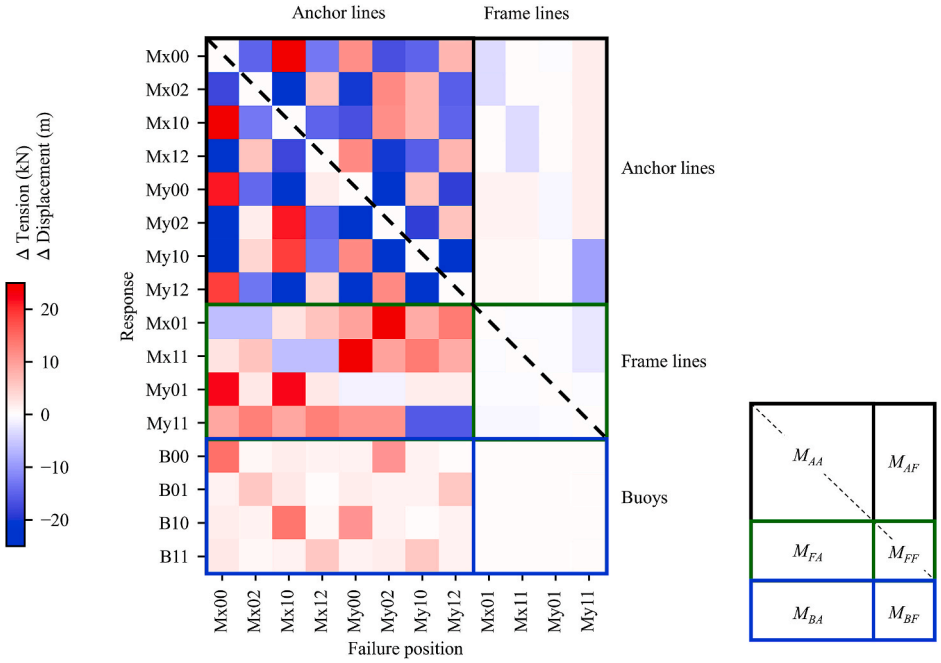

Fig. 11. The change of tension in mooring lines and the movements of buoys with respect to the different positions of mooring line breakages when current velocity is 0.5 m/s and $\theta = 0°$.

blocks, which are shown at the lower right of Fig. 11, indicate the influence of one component on others. For example, M_{AF} represents the influence on tensions in the anchor lines due to the frame line breakages. The influence of breakages at the two components and current directions will be discussed in Section 4.1.5.

An example of the displacement of the fish farm can be seen in Fig. 12. When the anchor line Mx00 breaks, the whole fish farm is no longer symmetric with respect to X-axis. Thus, the tensions among the remaining mooring lines are no longer symmetric, as shown in Fig. 9. The first column of Fig. 11 shows the changes of tension in the remaining mooring lines after anchor line Mx00 breaks. It is seen that the tension in anchor line Mx10, which is parallel to the broken anchor line Mx00, increases 32 kN (1.4 times of its tension under intact condition). Similar observations were also reported by Tang et al. (2020) and Yang et al. (2020). According to Tang et al. (2020), the tension in the remaining anchor line can increase up to 1.75 times due to mooring line breakage under the condition with the current velocity of 1.0 m/s and irregular waves corresponding to a 50-year return period. In addition, tensions in anchor lines My00 and My12 are clearly increased as well, which is similar to the results reported by Tang et al. (2020) and Yang et al. (2020). Except for these three anchor lines, the tensions in the remaining anchor lines are reduced after anchor line Mx00 breaks. As for the frame lines, the tensions in three of the frame lines increase, and tensions in only one frame line reduces. Generally, the changes of tension among the frame lines are smaller than those in anchor lines. The other columns, which indicate the influence of breakages at different mooring lines, will be discussed in Section 4.1.4.

4.1.3. *Movement of buoys after mooring line breakage*

As shown in Fig. 12, due to the breakage of anchor line Mx00, the buoy B00 moves towards the X+ direction significantly. However, the other three buoys have negligible movements as their constraining structures are still intact. The movements of buoys are also shown in Fig. 11. The movement of a buoy is calculated as the distance between the buoy before and after one of the mooring lines breaks. As the distance is non-negative, the colour for the movement of buoys is always red. According to the first column in Fig. 11, the movements of B00 is clearly larger than the other three buoys.

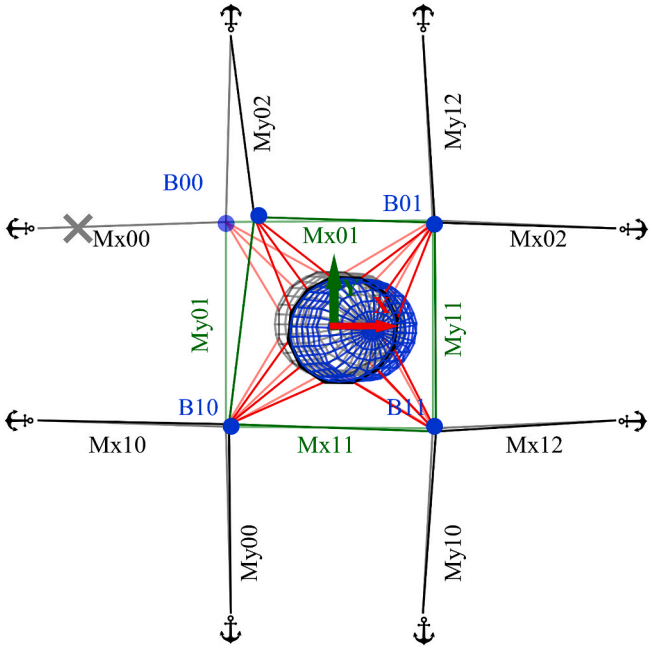

Fig. 12. Top view of the single-cage fish farm when the anchor line Mx00 breaks, current velocity is 0.5 m/s and $\theta = 0°$.

4.1.4. Influence of breakages at different mooring lines

If one of the mooring lines breaks, the fish farm with the remaining components is most likely geometrically asymmetric, and the tension distribution among the remaining mooring lines may lose the symmetric characteristics as shown in Section 4.1.1. The breakages at different mooring lines usually cause different tension distributions, but symmetric characteristics of the changes in the structural responses can still be observed between different cases. The different columns in Fig. 11 represent the changes in mooring line tensions and buoy movements caused by the breakages at different mooring lines when $\theta = 0°$. The dashed diagonal line for M_{AA} and M_{FF} represents the influence of the broken mooring to itself. Since only the responses of the remaining components are discussed in the present study, the values on this diagonal line are set to zero. Symmetric values with respect to this diagonal line can be observed from M_{AA}. For example, M_{AA} (3,1) = M_{AA} (1,3), M_{AA} (4,2) = M_{AA} (2,4) and M_{AA} (7,8) = M_{AA} (8,7), where the pair numbers in brackets are the index for the row number and the column number. Taking M_{AA} (3,1) = M_{AA} (1,3) for instance, the symmetric values imply that when $\theta = 0°$, the influence from the broken Mx00 on Mx10 is equivalent to the influence from the broken Mx10 to Mx00. This is because of the symmetric characteristics of the intact fish farm, as discussed in Section 4.1.1.

Whichever anchor line breaks, the number of mooring lines with increased tension compared to intact condition is the same. When one of the anchor lines breaks, there are always three anchor lines and three frame lines experiencing increased tensions. More specifically, the tensions in one of the remaining anchor lines which are parallel to the broken anchor line will increase, and the tension in two of the remaining anchor lines which are perpendicular to the broken anchor line will increase. As for the frame lines, the tension always decreases in the frame lines, which is parallel with and directly connected to the broken anchor line, and increases in the rest of the frame lines. However, when one of the frame lines breaks, the changes of tensions in the remaining mooring lines are relatively insignificant. Hereby, the colours in M_{AF} and M_{FF} are lighter than those in M_{FA} and M_{AA}, as shown in Fig. 11.

Whichever anchor line breaks, the buoy which is directly connected to the broken anchor line has the most significant movement. This is because the constraint which holds this buoy at the desired position disappears due to the breakage of the anchor line. For the other three buoys, the constraints still work similarly to the condition that before the breakage happens. Thus, the movement of the buoys that are not directly connected to the broken anchor line is negligible. However, when one of the frame lines breaks, the movements of all buoys are negligible. Thus, the colours in M_{BF} are almost white, as shown in Fig. 11.

4.1.5. Influence of current directions

As shown in Fig. 11, the colours in the last four columns corresponding to the breakage of frame lines (*i.e.*, M_{AF}, M_{FF} and M_{BF}) are clearly lighter than the colours in the first eight columns corresponding to the anchor lines breakage cases (*i.e.*, M_{AA}, M_{FA} and M_{BA}). These lighter colours mean that the influence on the mooring system caused by frame lines breakages is smaller than those caused by anchor lines breakages. Thus, it can be considered that frame lines are less crucial than anchor lines regarding the robustness of the fish farm. In order to compare the importance of the two components, *i.e.*, anchor lines and frame lines, the root-mean-square (RMS) value of the changes in the responses is introduced as an indicator. The RMS is calculated based on the values in each block, as shown in Fig. 11. The values in each block can be considered as a matrix. The RMS value of each matrix can reflect the averaged changes of tensions in the remaining mooring lines or the averaged movements of buoys due to breakages of the two components, and is calculated as follows:

$$\|M\|_{RMS} = \left(\frac{1}{m \times n} \sum_{i=1}^{n} \sum_{j=1}^{m} (a_{ij})^2 \right)^{1/2} \tag{9}$$

where m and n are the row and column numbers for the matrices, respectively. a_{ij} is the value shown by the colour in Fig. 11.

Fig. 13 presents the RMS value for the six matrices with respect to different current directions. Due to the symmetric characteristics discussed from Sections 4.1.1 to 4.1.4, the RMS is only given for 0°–90°. In this figure, all the lines are nearly horizontal, which means that the averaged changes in the responses due to mooring line breakages at different components exhibit little sensitivity to the current direction. In addition, the solid lines are always higher than the dashed lines. This implies that the influence caused by the anchor line breakages is always larger than those caused by the frame line breakages. Meanwhile, the breakages at anchor lines are always easier to notice than those at frame lines, as M_{BA} is always larger than M_{BF}.

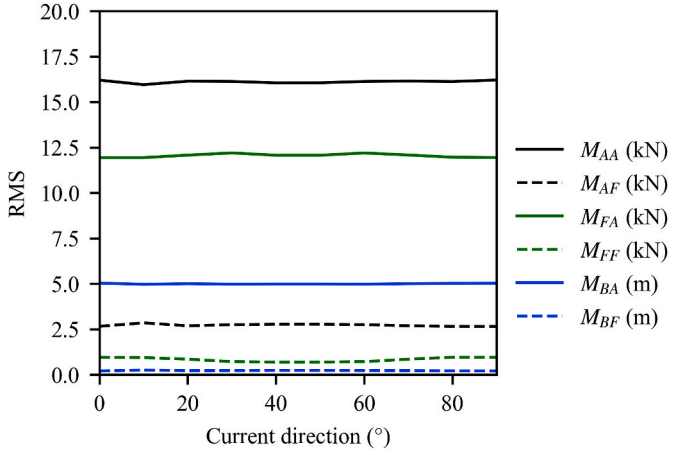

Fig. 13. The RMS for matrices with respect to different current directions.

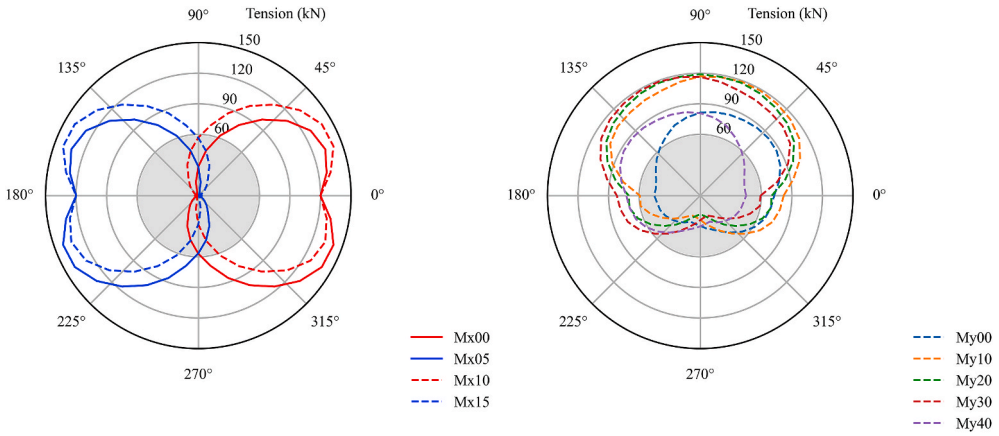

Fig. 14. Tension distribution in anchor lines under different current directions when the mooring system is in intact condition and current velocity is 0.5 m/s. The grey shadow represents pre-tension in anchor lines.

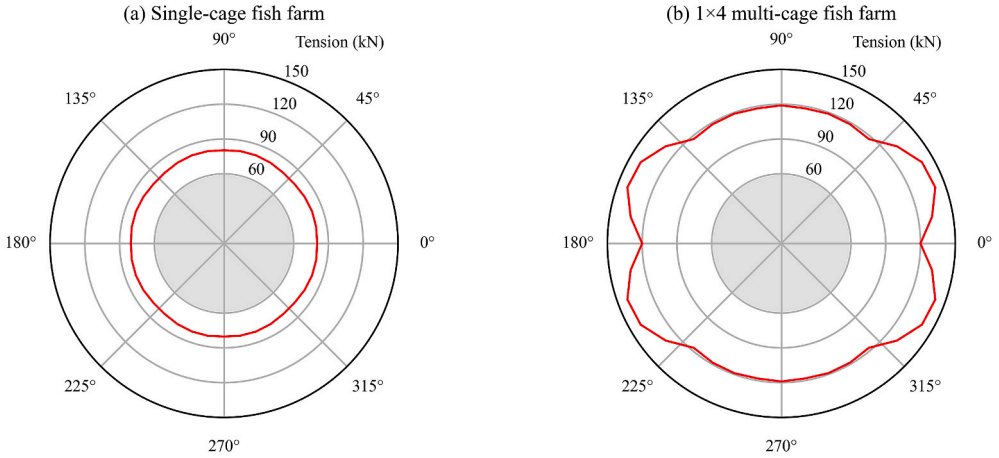

Fig. 15. Extreme tension in mooring lines under different current directions when the mooring system is in intact condition and current velocity is 0.5 m/s. The grey shadow represents pre-tension in anchor lines.

4.2. Structural responses of the multi-cage fish farm due to mooring line breakage

4.2.1. Tension distribution before mooring line breakage

Fig. 14 presents the tension distribution before mooring line breakage with respect to different current directions. For the tensions in the "My–" anchor lines, only half of them are plotted in the right subplot of Fig. 14 to make this figure readable. The tensions in the other half mooring lines can be obtained based on the symmetry, similar to the single-cage fish farm. Moreover, the left subplot in Fig. 14 shows that zero-tension appears in "Mx" anchor lines when the angle between the current direction and the longest axis of this 1 × 4 multi-cage fish farm is less than 45°. Under these current directions, the anchor lines with small tension may become slack and have abrasions with the seabed. According to Cardia and Lovatelli (2015), these abrasions can rapidly abrade the anchor lines to a dangerous condition and should be avoided in the design. The use of floats, attached close to the lower end of the anchor lines, can reduce the possibility of these abrasions.

Fig. 15 shows the extreme tension in anchor lines under different current directions. The extreme tension represents the largest tension among all the mooring lines. In this 1 × 4 multi-cage fish farm, the maximum extreme tension (around 140 kN) is almost 2.3 times of the pre-tension (around 60 kN), and it is much higher than that in the single-cage fish farm (around 80 kN) due to higher total environmental loads. For example, the total drag force on the four fish cages is around 211 kN when $\theta = 0°$, which is three times larger than that on the single fish cage (72 kN). The maximum extreme tension in this 1 × 4 multi-cage fish farm occurs when the angle between the current direction and the longest axis of the fish farm is 20°–30°. However, the extreme tension is not sensitive to the current direction in the single-cage fish farm. According to the explanation by Sim et al. (2021), the layout of the two fish farms together with the wake effect can cause different reactions of extreme tension under different current directions. Due to the wake effect, the current velocity is reduced after the current flowing through a fish cage (Zhao et al., 2015). The reduced current velocity can lead to a smaller drag force on these fish cages which locate in the wake region of the upstream cages. When the current direction increases from 0° to 90°, the total drag force on the four fish cages first increases from the smallest value (around 211 kN) at 0° to around 320 kN at 30°, and then remains at the maximum value. It should be noted that the drag force is the maximum does not necessarily mean that the extreme tension in the mooring system is the maximum, as the number of effective anchor lines also changes with the current direction. The effective anchor lines are the main lines that hold the fish farm in position. For example, when $\theta =$ 0°, Mx00 and Mx10 are the main effective anchor lines to hold this 1 × 4 fish farm in position. When $\theta = 90°$, Myi0 ($i = 0, 1, 2, 3$ and 4) are the main effective anchor lines. Under the same total drag force, more effective anchor lines can lead to smaller extreme tension in the mooring system. Due to the total drag force and the number of effective anchor lines, the highest tension happens when the current direction is around 20°–30°. For other current directions (90°–360°), similar observations can be seen due to the geometric symmetry of this fish farm. As for the

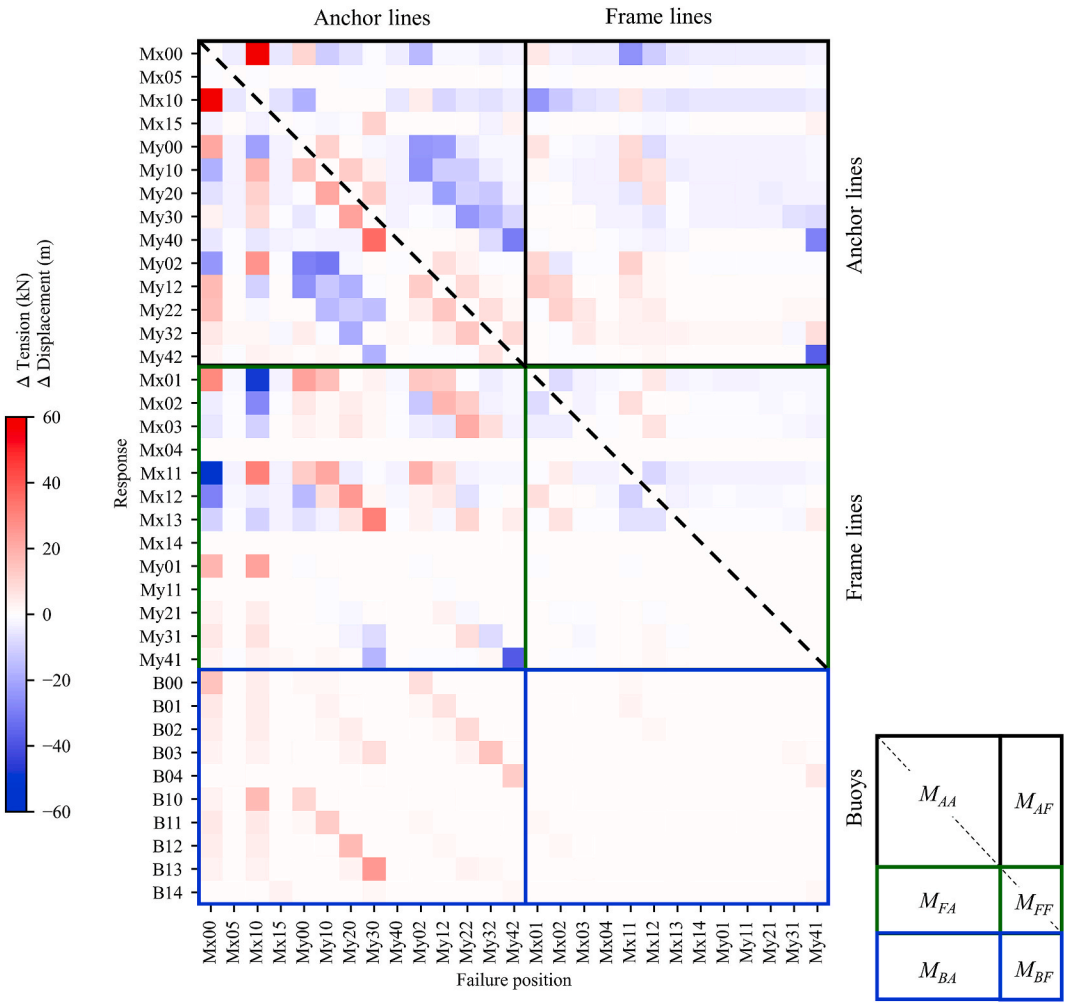

Fig. 16. The changes of tensions in mooring lines and the movements of buoys in the 1 × 4 multi-cage fish farm with respect to the different positions of mooring line breakages, when current velocity is 0.5 m/s and $\theta = 30°$.

single-cage fish farm, the total drag forces and effective anchor lines do not change with the current directions. Thus, the extreme tension in this single-cage fish farm is always around 80 kN.

4.2.2. *Tension distribution and movement of buoys after mooring line breakage*

Fig. 16 shows the tension distribution and the movement of buoys after one of the mooring lines breaks when the current velocity is 0.5 m/

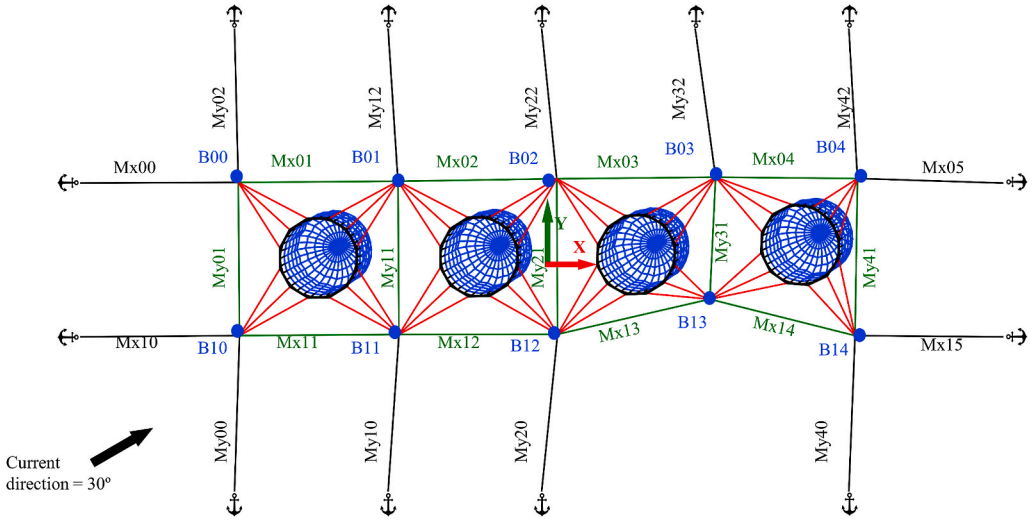

Fig. 17. Top view of the 1 × 4 multi-cage fish farm when the anchor line My30 breaks, current velocity is 0.5 m/s and θ = 30°.

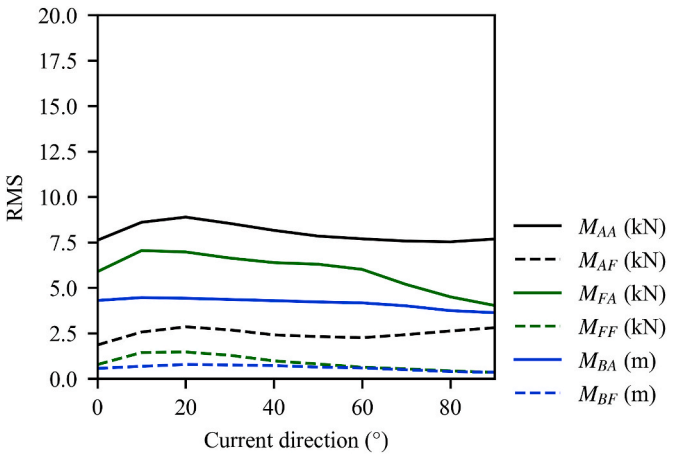

Fig. 18. The RMS for matrices under different current directions.

s and θ = 30°. The symmetric characteristics which are discussed in Fig. 11 cannot be observed in this figure, as the current is not along the axis of symmetry for this 1 × 4 multi-cage fish farm. Usually, the breakages at different mooring lines can cause different tension increment or decrement in the remaining mooring lines. However, some mooring lines, *e.g.*, Mx05, Mx04 and Mx14, are always white, as shown in Fig. 16. That white colour means that whichever mooring lines break, the tensions in these mooring lines are always the same as theirs under intact condition. Actually, these mooring lines are zero-tension and slack under the intact condition when θ = 30°. As the remaining mooring lines can still hold the whole fish farm, these zero-tension mooring lines are still slack. Thus, the tensions in these mooring lines have no change after mooring line breakages.

Fig. 17 shows the top view of this 1 × 4 multi-cage fish farm after anchor line My30 breaks when current velocity is 0.5 m/s and $\theta = 30°$. It can be observed that the buoy B13 have a significant movement towards Y+ direction, and the other buoys have relatively smaller movements. The distances of these movements are shown in Fig. 16.

4.2.3. Influence of current directions

As shown in Fig. 18, the influence due to frame line breakages is less serious than that due to anchor line breakages. Unlike the single-cage fish farm, for this 1 × 4 multi-cage fish farm, the influence on the changes of tensions in the remaining mooring lines due to mooring line breakages is dependent on the current direction. When $20° < \theta < 30°$, the influence on the changes of tensions in the remaining mooring lines due to anchor line breakages is strongest among all current directions. When $20° < \theta < 30°$, the extreme tension is also the maximum under intact condition, as shown in Fig. 15. This implies that the influence is related to the extreme tensions before mooring line breakages. If the extreme tension in the intact condition is high, a stronger influence on the changes of the tensions is expected after mooring line breakages. As for the influence on the movements of buoys, M_{BA} is always larger than M_{BF}, and both are independent of current directions.

Table 3
Fish farm with grid mooring system.

Layout of fish farm	Number of fish cage	Number of anchor line	Number of anchor line per fish cage
1 × 1	1	8	8
1 × 4	4	14	3.5
1 × 8	8	22	2.75
2 × 2	4	12	3
2 × 3	6	14	2.33
2 × 4	8	16	2
2 × 6	12	20	1.66

4.3. Mooring system design consideration

Usually, a fish farm consists of several fish cages, and these fish cages are arranged in arrays using a grid-like mooring system. According to Cardia and Lovatelli (2015), the most common layouts of a fish farm are 2 × 3, 2 × 4 and 2 × 6. During the design of a mooring system, the ratio between the number of fish cages and the number of anchor lines is a useful indicator to measure the robustness of the fish farm. As shown in Table 3, a fish farm with a small number of fish cage usually has a relatively larger number of anchor lines per fish cage. A larger number of anchor lines per fish cage is preferred in an exposed site, as the position of the fish farm can be kept more securely. As shown in Fig. 19, the maximum increment of tension in the single-cage fish farm is less than half of that in the 1 × 4 multi-cage fish farm. Thus, the fish farm with a larger number of anchor lines per fish cage has a higher chance to sustain the fish farm after one of the mooring lines breaks. While in a sheltered site, a fish farm with more fish cages and small anchor lines per fish cage is preferable, as it requires relatively fewer anchors and mooring lines, and subsequently lower installation costs.

In some cases, additional anchor lines are required to reinforce the mooring system, particularly in an exposed site. Fig. 19 shows the relationship between the maximum tension increment in the mooring system and the maximum buoy movement after one mooring line breaks. For example, one point in the left scatterplot is extracted based on the first column of Fig. 10. The X-value in the scatter plot corresponds to the maximum movement, which is from B00, and the Y-value corresponds to the maximum tension increment, which is from MX10. The figure summarises the results for all the cases with different breakage situations. Due to the symmetry of the fish farm set-up, the scatter plots only include results for current directions of $0° = \theta \leq 90°$. Thus, there are 10 × 12 = 120 points in the left subplot and 10 × 27 = 270 points in the right subplot. According to the right subplot, the breakages at the "Mx" anchor lines can lead to a higher tension increment in the mooring system, compared to the breakages at the "My" anchor lines. In order to reinforce the mooring system, additional anchor lines should be added as a backup for the "Mx" anchor lines. According to Figs. 15 and 18, When $20° < \theta < 30°$, the extreme tension in the mooring system is the maximum, and the influence of mooring line breakages is also the strongest. Thus, the most effective way to improve the security and reliability of this 1x4 multi-cage fish farm is to add additional anchor lines in the four corners, as shown in Fig. 20.

4.4. Observations during operation

The breaking strength for the considered anchor lines (50 mm three-strand Polysteel rope) in this study is around 360 kN, which is larger than the extreme tension (around 220 kN) in the remaining mooring lines of the 1x4 multi-cage fish farm after one of the mooring lines breaks. Thus, the mooring system should not have progressive collapse under operational conditions. However, if this breakage is not detected, the damaged mooring system may not be able to keep the fish farm in position during higher currents and waves. Consequently, the undetected mooring line breakage can lead to a structural collapse and fish escape, which is a serious accident. As reported by Føre and Thorvaldsen (2021), the most serious fish escape in the period of 2010–2018 occurs because of the breakages in the mooring system. In order to avoid this serious fish escape, one way is to increase the conservativeness during the design, which means to increase the breaking strength of anchor lines by using stronger material or a larger diameter of the ropes. This improvement can increase the initial financial investment for a fish farm. Another way is to monitor the positions of buoys during or after in-situ operations.

According to NS9415 (Standards Norway, 2009), the regular inspections of a fish farm only emphasize the structural integrity of netting and floating collar. Monitoring the positions of buoys has not been given enough attention. However, based on the results from Sections 4.1.1 and

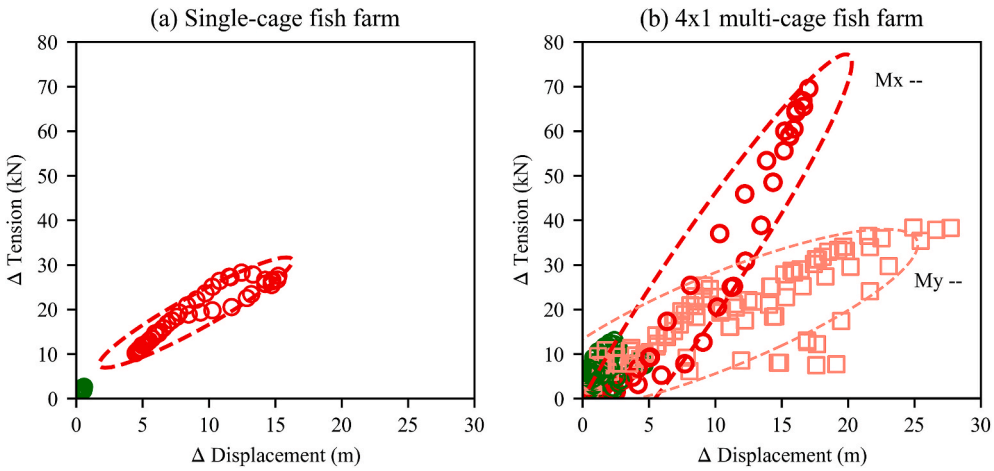

Fig. 19. The extreme change of tension among mooring lines after one of mooring lines breaks. The green colour represents the conditions when frame line breaks. For subplot (a), the red circles represent the conditions when one anchor line breaks. For subplot (b), the red circles represent the conditions when one "Mx" anchor line breaks, and the light red squares represent the conditions when one "My" anchor line breaks. Confidence ellipse with 95 % confidence is plotted for these anchor line breaks. (For interpretation of the references to colour in this figure legend, the reader is referred to the Web version of this article.)

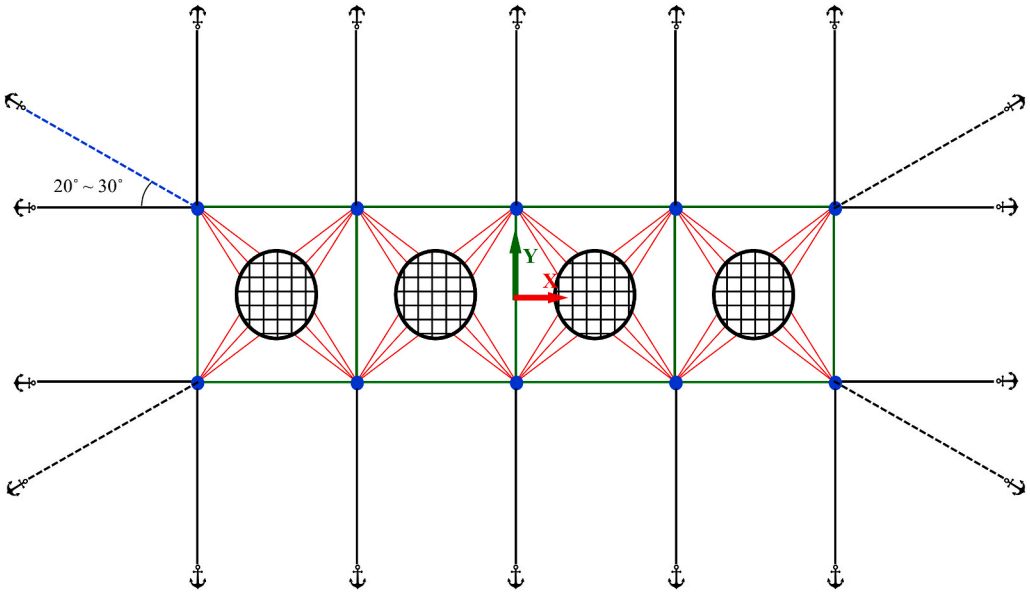

Fig. 20. The 1 × 4 multi-cage fish farm with additional corner mooring lines.

4.1.2, the displacements of the buoys can act as a good indicator to detect the mooring line breakage. As shown in Fig. 19, the tension increment in the mooring system has a strong correlation with the movement of buoys. If one of the buoys is observed to have a large movement, it is most likely that one of the mooring lines breaks. The present analysis shows that the broken mooring line is most likely the one directly connected to the buoy with the largest movement.

In Norway, most of the in-situ operations in a fish farm are handled by various auxiliary equipment, such as net cleaners, buoy ropes for crowding of fish, tarpaulins for parasite treatment and netting for fish handing. It may not be easy to notice the movement of buoys while the equipment operators are working. From a practical point of view, it is useful to install a Global Positioning System (GPS) device on each buoy. The GPS device can record the locations of buoys and send the information back to the operators and administrators. Based on the movements of buoys, a warning system to detect mooring line breakages can be established. According to the previous studies by Zhao et al. (2019) and Bi et al. (2020), a warning system for mooring line breakages can be established through a deep learning method based on more simulations as presented in the present study. By then, the breakages in the mooring system can be quickly and automatically discovered and precisely located, and the tension distribution in the remaining mooring system can be predicted with seconds. The administrator can make a corresponding decision based on these predictions, such as: (1) stop the operation immediately or (2) continue the operation and repair the damaged mooring line later. With more data training, the autonomous fish farming system for early prediction proposed by Yang et al. (2020b) can also be achieved in the future.

5. Conclusions

In the present study, the structural responses of the two fish farms, *i.e.*, a single-cage fish farm and a 1 × 4 multi-cage fish farm, are comprehensively analysed with respect to combinations of mooring line breakages and current directions. Due to the symmetry of the two fish farms, symmetric results are shown and discussed. Based on these results, suggestions to improve the design of the mooring system are given. It is also recommended to monitor the positions of buoys during operation to detect the mooring line breakages. Besides, the following conclusions are drawn from this study:

1. Breakage at one mooring line is unlikely to cause a progressive collapse of the fish fam under operational conditions, such as current velocity <0.5 m/s. The extreme tension in the remaining mooring

lines of the 1x4 multi-cage fish farm is around 220 kN after one of the mooring lines breaks under operational condition. This value is 3.6 times larger than the pre-tension and 60 % of the designed breaking strength. However, mooring line breakages may cause structural collapse and fish escape when the current and waves become stronger, if the breakages remain undetected.

2. Monitoring the positions of buoys during and after in-situ operations is recommended and could be emphasised in the operational handbook, since mooring line breakages can be discovered and located from the movement of buoys. The broken mooring line is usually directly connected to the buoy with the largest movement.
3. The increment of tension in the mooring system due to mooring line breakages has a strong positive correlation with the movement of buoys. Based on the displacement of the buoys with the largest movement, the maximum tension increment in the mooring system can be estimated. This estimation can help the operators of fish farms to decide whether or not to repair the damaged mooring line immediately.

CRediT authorship contribution statement

Hui Cheng: Conceptualization, Methodology, Software, Validation, Formal analysis, Investigation, Data curation, Writing – original draft, Writing – review & editing, Visualization. **Lin Li:** Conceptualization, Methodology, Supervision, Writing – review & editing. **Muk Chen Ong:** Conceptualization, Methodology, Resources, Writing – review & editing, Supervision, Project administration. **Karl Gunnar Aarsæther:** Conceptualization, Methodology, Software, Writing – review & editing. **Jaesub Sim:** Investigation, Visualization, Writing – review & editing.

Declaration of competing interest

The authors declare that they have no known competing financial interests or personal relationships that could have appeared to influence the work reported in this paper.

References

AKVA group, 2020. Pen Farming Aquaculture Catalogue. https://cdn2.hubspot.net/hubfs/4074933/Produktark/Cage%20Farming%20Aquaculture%20Cage%20Cat_E%20-%203_1-18.pdf.

Antonutti, R., Peyrard, C., Incecik, A., Ingram, D., Johanning, L., 2018. Dynamic mooring simulation with Code_Aster with application to a floating wind turbine. Ocean Eng. 151, 366–377. https://doi.org/10.1016/j.oceaneng.2017.11.018.

Berstad, A.J., Tronstad, H., Ytterland, A., 2004. Design rules for marine fish farms in Norway: calculation of the structural response of such flexible structures to verify structural integrity. In: 23rd International Conference on Offshore Mechanics and Arctic Engineering, Volume 3. Presented at the ASME 2004 23rd International Conference on Offshore Mechanics and Arctic Engineering. ASMEDC, pp. 867–874. https://doi.org/10.1115/OMAE2004-51577. Vancouver, British Columbia, Canada.

Bi, C.-W., Zhao, Y.-P., Dong, G.-H., Zheng, Y.-N., Gui, F.-K., 2014. A numerical analysis on the hydrodynamic characteristics of net cages using coupled fluid–structure interaction model. Aquacult. Eng. 59, 1–12. https://doi.org/10.1016/j.aquaeng.2014.01.002.

Bi, C.-W., Zhao, Y.-P., Sun, X.-X., Zhang, Y., Guo, Z.-X., Wang, B., Dong, G.-H., 2020. An efficient artificial neural network model to predict the structural failure of high-density polyethylene offshore net cages in typhoon waves. Ocean Eng. 196 https://doi.org/10.1016/j.oceaneng.2019.106793, 106793.

Cardia, F., Lovatelli, A., 2015. Aquaculture Operations in Floating HDPE Cages: a Field Handbook. Food and Agriculture Organization of the United States, Rome. http://www.fao.org/3/i4508e/I4508E.pdf.

Cheng, H., Aarsæther, K.G., Li, L., Ong, M.C., 2020a. Numerical study of a single-point mooring gravity fish cage with different deformation-suppression methods. J. Offshore Mech. Arctic Eng. 142, 41301. https://doi.org/10.1115/1.4046115.

Cheng, H., Li, L., Aarsæther, K.G., Ong, M.C., 2020b. Typical hydrodynamic models for aquaculture nets: a comparative study under pure current conditions. Aquacult. Eng. 90 https://doi.org/10.1016/j.aquaeng.2020.102070, 102070.

Cheng, H., Ong, M.C., Li, L., Chen, H., 2021. Development of a coupling algorithm for fluid-structure interaction analysis of flexible nettings in fluid. Ocean Eng. Submitted for publication.

Endresen, P.C., Birkevold, J., Føre, M., Fredheim, A., Kristiansen, D., Lader, P., 2014. Simulation and validation of a numerical model of a full aquaculture net-cage system, in: volume 7: ocean space utilization; professor Emeritus J. Randolph paulling Honoring symposium on ocean technology. In: Presented at the ASME 2014 33rd International Conference on Ocean, Offshore and Arctic Engineering. American Society of Mechanical Engineers. https://doi.org/10.1115/OMAE2014-23382. San Francisco, California, USA, p. V007T05A006.

Endresen, P.C., Føre, M., Fredheim, A., Kristiansen, D., Enerhaug, B., 2013. Numerical modeling of wake effect on aquaculture nets, in: volume 3: materials technology; ocean space utilization. In: Presented at the ASME 2013 32nd International Conference on Ocean, Offshore and Arctic Engineering. American Society of Mechanical Engineers. https://doi.org/10.1115/OMAE2013-11446. Nantes, France, p. V003T05A027.

Enerhaug, B., Føre, M., Endresen, P.C., Madsen, N., Hansen, K., 2012. Current loads on net panels with rhombic meshes. In: Ocean Space Utilization; Ocean Renewable Energy. Presented at the ASME 2012 31st International Conference on Ocean, Offshore and Arctic Engineering, ume 7. American Society of Mechanical Engineers, pp. 49–60. https://doi.org/10.1115/OMAE2012-83394. Rio de Janeiro, Brazil.

FAO, 2020. The State of World Fisheries and Aquaculture 2020: Sustainability in Action, the State of World Fisheries and Aquaculture (SOFIA). FAO. https://doi.org/10.4060/ca9229en. Rome, Italy.

Fredheim, A., Reve, T., 2018. Future prospects of marine aquaculture. In: OCEANS 2018 MTS/IEEE Charleston. Presented at the OCEANS 2018 MTS/IEEE Charleston, pp. 1–8. https://doi.org/10.1109/OCEANS.2018.8604735.

Fredriksson, D.W., DeCew, J., Lader, P., Volent, Z., Jensen, Ø., Willumsen, F.V., 2014. A finite element modeling technique for an aquaculture net with laboratory measurement comparisons. Ocean Eng. 83, 99–110. https://doi.org/10.1016/j.oceaneng.2014.03.005.

Gansel, L.C., McClimans, T.A., Myrhaug, D., 2012. The Effects of Fish Cages on Ambient Currents. J. Offshore Mech. Arct. Eng, p. 134. https://doi.org/10.1115/1.4003696.

Gutiérrez-Romero, J.E., Lorente-López, A.J., Zamora-Parra, B., 2020. Numerical analysis of fish farm behaviour in real operational conditions. Ships Offshore Struct. 15, 737–752. https://doi.org/10.1080/17445302.2019.1671674.

Halwart, M., Soto, D., Arthur, J.R. (Eds.), 2007. Cage Aquaculture: Regional Reviews and Global Overview, FAO Fisheries Technical Paper. FAO, Rome. http://www.fao.org/docrep/pdf/010/a1290e/a1290e.pdf.

Høyli, R., 2016. Assessing the Risk of Escape from Marine Fish Farms - Improving Data Collection Strategies and Development of Risk Indicators (Master Thesis). UiT The Arctic University of Norway, Tromsø, Norway. https://hdl.handle.net/10037/9633.

Johansen, V., 2007. Modelling of flexible slender systems for real-time simulation and control applications (Doctoral thesis). Norwegian University of Science and Technology, Trondheim, Norway. http://hdl.handle.net/11250/237621.

Kristiansen, T., Faltinsen, O.M., 2012. Modelling of current loads on aquaculture net cages. J. Fluid Struct. 34, 218–235. https://doi.org/10.1016/j.jfluidstructs.2012.04.001.

Moe Føre, H., Thorvaldsen, T., 2021. Causal analysis of escape of Atlantic salmon and rainbow trout from Norwegian fish farms during 2010–2018. Aquaculture 532. https://doi.org/10.1016/j.aquaculture.2020.736002, 736002.

Moe Føre, H., Thorvaldsen, T., Astrid, B., Eivind, L., Fagertun, J.T., 2019. Tekniske Årsaker Til Rømming Av Oppdrettslaks Og Regnbueørret for Perioden 2014-2018 (Report). SINTEF Ocean AS. http://hdl.handle.net/11250/2601601.

Norwegian Directorate of Fisheries, 2005. Aquaculture Act [WWW Document]. URL. http://fiskeridir.no/English/Aquaculture/Aquaculture-Act. accessed 11.22.20.

Priour, D., 2013. A Finite Element Method for Netting: Application to Fish Cages and Fishing Gear, first ed. Springer Netherlands, Dordrecht. https://doi.org/10.1007/978-94-007-6844-4.

Priour, D., 1999. Calculation of net shapes by the finite element method with triangular elements. Commun. Numer. Methods Eng. 15, 755–763. https://doi.org/10.1002/(SICI)1099-0887(199910)15:10<755::AID-CNM299>3.0.CO;2-M.

Reite, K.-J., Føre, M., Aarsæther, K.G., Jensen, J., Rundtop, P., Kyllingstad, L.T., Endresen, P.C., Kristiansen, D., Johansen, V., Fredheim, A., 2014. FHSIM — Time Domain Simulation of Marine Systems. Presented at the ASME 2014. In: 33rd International Conference on Ocean, Offshore and Arctic Engineering. American Society of Mechanical Engineers Digital Collection. https://doi.org/10.1115/OMAE2014-23165. San Francisco, California, USA.

Shen, Y., Greco, M., Faltinsen, O.M., 2019a. Numerical study of a well boat operating at a fish farm in current. J. Fluid Struct. 84, 77–96. https://doi.org/10.1016/j.jfluidstructs.2018.10.006.

Shen, Y., Greco, M., Faltinsen, O.M., 2019b. Numerical study of a well boat operating at a fish farm in long-crested irregular waves and current. J. Fluid Struct. 84, 97–121. https://doi.org/10.1016/j.jfluidstructs.2018.10.007.

Shen, Y., Greco, M., Faltinsen, O.M., Nygaard, I., 2018. Numerical and experimental investigations on mooring loads of a marine fish farm in waves and current. J. Fluid Struct. 79, 115–136. https://doi.org/10.1016/j.jfluidstructs.2018.02.004.

Sim, J., Cheng, H., Aarsæther, K.G., Li, L., Ong, M.C., 2021. Numerical investigation on the cage-to-cage wake effect: a case study of a 4x2 cage array. J. Offshore Mech. Arctic Eng. https://doi.org/10.1115/1.4049831.

Skjong, S., Reite, K.J., Aarsæther, K.G., 2021. Lumped, constrained cable modeling with explicit state-space formulation using an elastic version of Baumgarte stabilization. J. Offshore Mech. Arctic Eng. 143 https://doi.org/10.1115/1.4050422.

Standards Norway, 2009. NS 9415.E Marine Fish Farms—Requirements for Design. in: Dimensioning, Production, Installation and Operation. Standards Norway. https://www.standard.no/en/webshop/productcatalog/productpresentation/?ProductID=402400.

Statistics Norway, 2020. Aquaculture [WWW Document]. URL. https://www.ssb.no/en/jord-skog-jakt-og-fiskeri/statistikker/fiskeoppdrett/aar/2020-10-29. accessed 11.22.20.

Su, B., Reite, K.-J., Føre, M., Aarsæther, K.G., Alver, M.O., Endresen, P.C., Kristiansen, D., Haugen, J., Caharija, W., Tsarau, A., 2019. A multipurpose framework for modelling and simulation of marine aquaculture systems. Presented at the ASME 2019. In: 38th

International Conference on Ocean, Offshore and Arctic Engineering. American Society of Mechanical Engineers Digital Collection. https://doi.org/10.1115/OMAE2019-95414. Glasgow, Scotland, UK.

Tang, H.-J., Yang, R.-Y., Huang, C.-C., 2019. Numerical modelling of the mooring line failure induced performance changes of a marine fish cage in irregular waves and currents. In: Presented at the ASME 2019 38th International Conference on Ocean, Offshore and Arctic Engineering. American Society of Mechanical Engineers Digital Collection. https://doi.org/10.1115/OMAE2019-95730.

Tang, H.-J., Yeh, P.-H., Huang, C.-C., Yang, R.-Y., 2020. Numerical study of the mooring system failure of aquaculture net cages under irregular waves and current. Ocean Eng. 216 https://doi.org/10.1016/j.oceaneng.2020.108110, 108110.

Thorvaldsen, T., Holmen, I.M., Moe, H.K., 2015. The escape of fish from Norwegian fish farms: causes, risks and the influence of organisational aspects. Mar. Pol. 55, 33–38. https://doi.org/10.1016/j.marpol.2015.01.008.

Thorvaldsen, T., Moe Føre, H., Tinmannsvik, R.K., Okstad, E.H., 2018. Menneskelige Og Organisatoriske Årsaker Til Rømming Av Oppdrettslaks Og Regnbueørret (Report). SINTEF Ocean AS. http://hdl.handle.net/11250/2577751.

Yang, R.-Y., Tang, H.-J., Huang, C.-C., 2020. Numerical modeling of the mooring system failure of an aquaculture net cage system under waves and currents. IEEE J. Ocean. Eng. 45, 1396–1410. https://doi.org/10.1109/JOE.2019.2941768.

Yang, X., Utne, I.B., Holmen, I.M., 2020a. Methodology for hazard identification in aquaculture operations (MHIAO). Saf. Sci. 121, 430–450. https://doi.org/10.1016/j.ssci.2019.09.021.

Yang, X., Utne, I.B., Sandøy, S.S., Ramos, M.A., Rokseth, B., 2020b. A systems-theoretic approach to hazard identification of marine systems with dynamic autonomy. Ocean Eng. 217 https://doi.org/10.1016/j.oceaneng.2020.107930, 107930.

Zhao, Y.-P., Bi, C.-W., Chen, C.-P., Li, Y.-C., Dong, G.-H., 2015. Experimental study on flow velocity and mooring loads for multiple net cages in steady current. Aquacult. Eng. 67, 24–31. https://doi.org/10.1016/j.aquaeng.2015.05.005.

Zhao, Y.-P., Bi, C.-W., Dong, G.-H., Gui, F.-K., Cui, Y., Guan, C.-T., Xu, T.-J., 2013a. Numerical simulation of the flow around fishing plane nets using the porous media model. Ocean Eng. 62, 25–37. https://doi.org/10.1016/j.oceaneng.2013.01.009.

Zhao, Y.-P., Bi, C.-W., Dong, G.-H., Gui, F.-K., Cui, Y., Xu, T.-J., 2013b. Numerical simulation of the flow field inside and around gravity cages. Aquacult. Eng. 52, 1–13. https://doi.org/10.1016/j.aquaeng.2012.06.001.

Zhao, Y.-P., Bi, C.-W., Sun, X.-X., Dong, G.-H., 2019. A prediction on structural stress and deformation of fish cage in waves using machine-learning method. Aquacult. Eng. 85, 15–21. https://doi.org/10.1016/j.aquaeng.2019.01.003.